

October 17, 1995

---

CONTRACT NAS8-38856

**Structural Damage  
Prediction and Analysis  
for Hypervelocity Impact**

---

**AIAA 92-1588**

**Properties of Largest  
Fragment Produced by  
Hypervelocity Impact of  
Aluminum Spheres with  
Thin Aluminum Sheets**

Prepared for:  
National Aeronautics and Space Administration  
George C. Marshall Space Flight Center  
Marshall Space Flight Center,  
Alabama 35812







**AIAA 92-1588**

**Properties of Largest Fragment  
Produced By Hypervelocity Impact  
of Aluminum Spheres With Thin  
Aluminum Sheets**

Andrew J. Piekutowski  
University of Dayton Research Institute  
Dayton, Ohio

**AIAA Space Programs  
and Technologies Conference  
March 24-27, 1992 / Huntsville, AL**



# PROPERTIES OF LARGEST FRAGMENT PRODUCED BY HYPERVELOCITY IMPACT OF ALUMINUM SPHERES WITH THIN ALUMINUM SHEETS

Andrew J. Piekutowski  
University of Dayton Research Institute  
300 College Park  
Dayton, Ohio 45469-0180

## ABSTRACT

Results of a series of hypervelocity impact tests are presented. In these tests, 1.275-g, 9.53-mm-diameter, 2017-T4 aluminum spheres were fired at normal incidence at eight thicknesses of 6061-T6 aluminum sheet. Bumper thickness to projectile diameter ( $t/D$ ) ratio ranged from 0.026 to 0.424. Nominal impact velocity was 6.7 km/s. Results of five tests using 6.35, 9.53, and 12.70-mm-diameter aluminum spheres and other aluminum alloy bumpers are also given. A large chunky fragment of projectile was observed at the center of the debris clouds produced by the impacts. The equivalent diameter of this large fragment ranged from 5.5 mm for the lowest  $t/D$  ratio to a minimum of 0.6 mm for the case where maximum breakup of the projectile occurred ( $t/D \sim 0.2$  to  $0.3$ ). When the  $t/D$  ratio was 0.42, numerous large flaky fragments were evenly distributed in the external bubble of bumper debris. Velocity of the large central fragments decreased continuously with increasing  $t/D$  ratio, ranging from about 99 percent to less than 80 percent of the impact velocity. The change in the velocity of small fragments spalling from the rear of the projectile was used to obtain a relationship showing a linear increase in the size of the central projectile fragment with decrease in the shock-induced stress in the projectile.

## NOMENCLATURE

D	diameter of projectile
H	height of largest fragment
T	thickness of largest fragment
$V_f$	velocity of largest fragment
$V_0$	impact velocity of projectile
$V_r$	expansion velocity of hemispherical shell of fragments from rear surface of projectile
$V_{r \text{ opt}}$	expansion velocity, $V_r$ , at optimum $t/D$ ratio
$d_f$	equivalent diameter of largest fragment
$d_{f \text{ opt}}$	equivalent diameter of largest fragment at optimum $t/D$ ratio
t	thickness of bumper sheet

## INTRODUCTION

Hypervelocity impacts of aluminum spheres with aluminum plates have been studied for more than 30 years. Most of these studies have been directed toward optimizing a spacecraft shield design against a particular threat, i.e., providing maximum protection with a minimum weight and space penalty. The optimum or most effective shield produced maximum breakup and dispersion of the threatening particle, thereby spreading the debris over a large area and inflicting minimal damage on the rear wall. Wilkinson's<sup>1</sup> penetration criterion, for example, assumes "that the front sheet completely fragments or vaporizes the incoming particle, and that no large solid fragments remain." Optimization of a shield design against a range of fragment sizes, e.g., the orbital debris environment, is not a simple task. Of particular concern is the situation where the impacting fragments overmatch or undermatch the shield. In either of these cases, complete breakup of the fragment and/or bumper does not occur.

A recent study of debris clouds produced by the impact of aluminum spheres with thin aluminum plates<sup>2</sup> has examined the behavior of non-optimum shields. In this study, a variety of quantitative data were obtained from multiple-exposure, orthogonal pair, flash radiographs of the debris clouds produced by the impacts. For cases where the bumper was overmatched, i.e., the projectile did not breakup completely, a large single fragment of projectile remained at the center of the debris cloud. When the projectile was overmatched, numerous large bumper fragments were distributed throughout the bubble of bumper debris. Both types of fragments pose a penetration threat to the rear wall of a double sheet structure. This paper provides quantitative data regarding the size and velocity of these large fragments for impacts at 6.7 km/s.

## EXPERIMENTAL DESIGN

Test results presented in this paper were obtained from tests performed for two sponsors, Martin Marietta Manned Space Systems and McDonnell Douglas Space Systems Company, and from range and/or equipment performance tests conducted by the University of Dayton Research Institute (UDRI). Appropriate recognition of support for each test is given in the radiographs of debris clouds as they are presented. All tests were performed in the UDRI Impact Physics Laboratory using a 50/20 mm, two-stage, light gas gun.

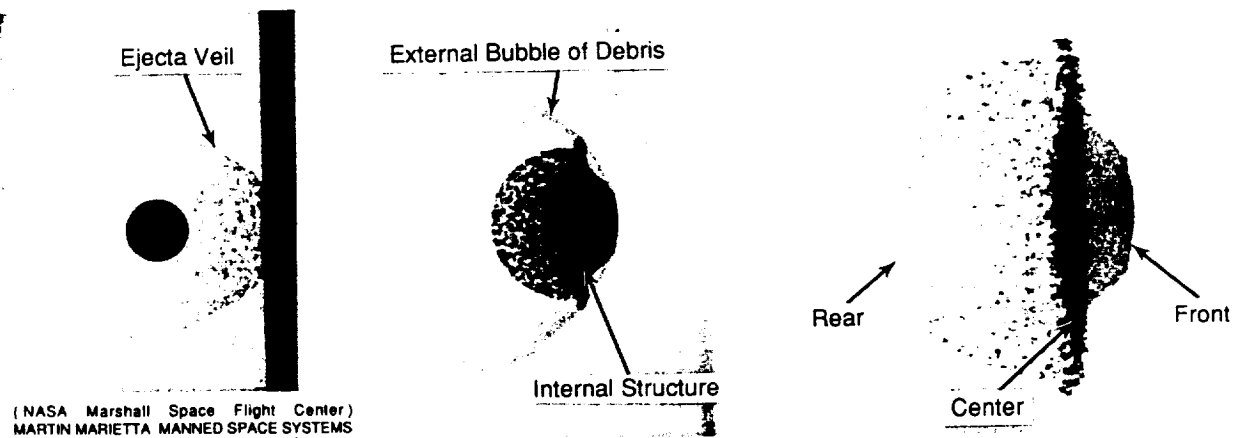


Fig. 3. Close up of radiograph shown in Fig. 2. Various morphological features and elements of the debris cloud structure are identified.



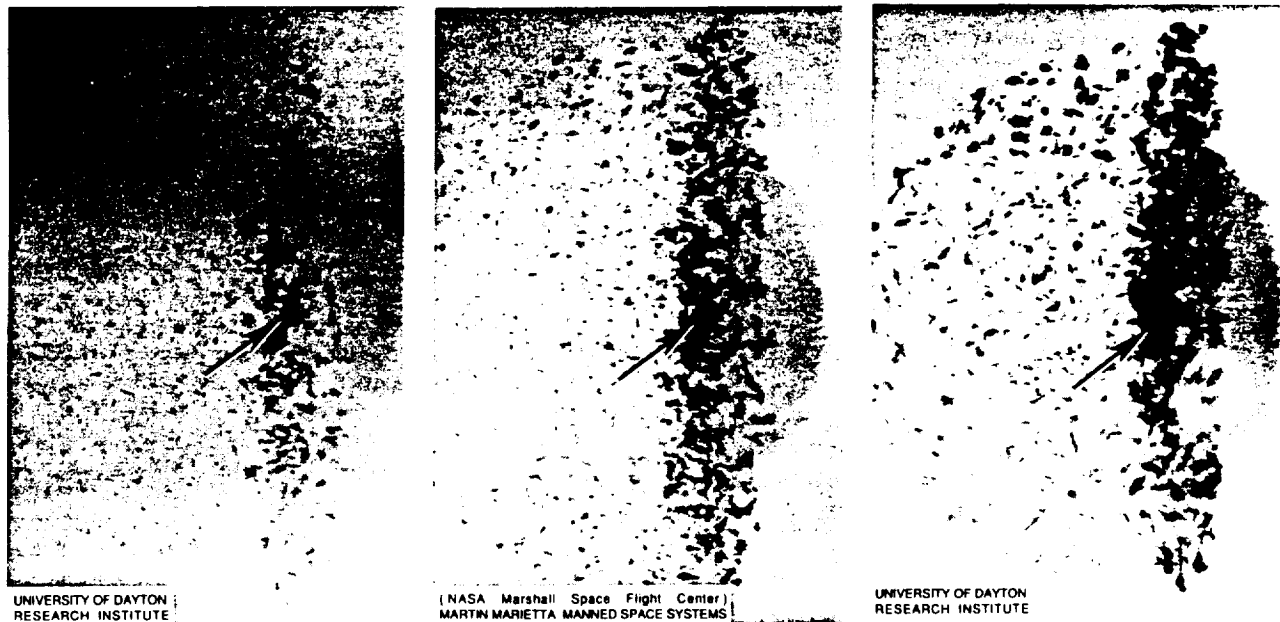


Fig. 7. Views of largest fragment produced by impacts of various diameters of aluminum spheres ( $t/D$  ratio held constant at 0.048). Left--6.35-mm-diameter, 0.373-g, 2017-T4 aluminum sphere; 0.302-mm-thick, 1100-0 aluminum bumper;  $V_0 = 6.67$  km/s. Center--9.53-mm-diameter, 1.275-g, 2017-T4 aluminum sphere; 0.465-mm-thick, 6061-T6 aluminum bumper;  $V_0 = 6.62$  km/s. Right--12.70-mm-diameter, 3.000-g, 2024-T3 aluminum sphere; 0.592-mm-thick, 6061-T6 aluminum bumper;  $V_0 = 6.26$  km/s.

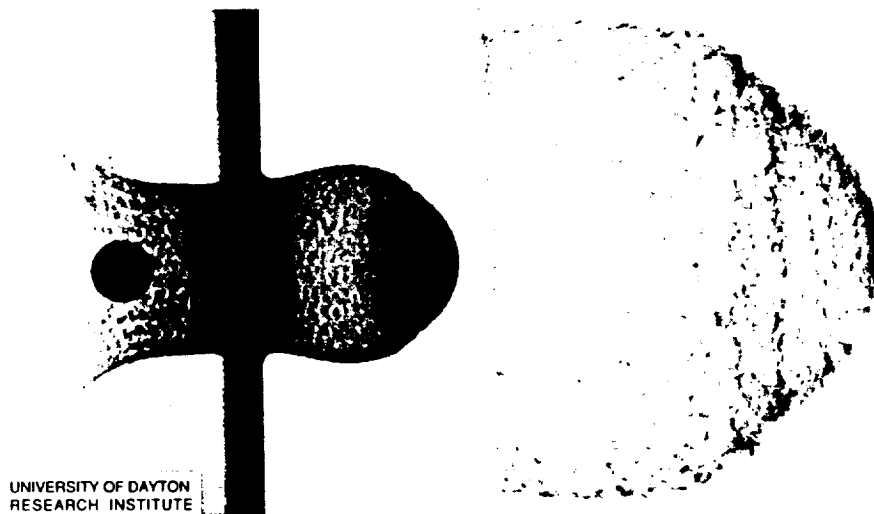


Fig. 8. View of external bubble of debris cloud produced by impact of 9.53-mm-diameter, 1.275-g, 2017-T4 aluminum sphere with a 4.039-mm-thick, 6061-T6 aluminum plate at 6.68 km/s.

view. In making the measurements, every precaution was taken to insure that the measurement was of the large fragment alone and not several overlapping fragments. To further insure the most reliable measurements were used to determine the volume of the largest fragment, the smaller of the two thickness measurements was used in the computation. The measured values of largest fragment height,  $H$ ; width,  $W$ ; and thickness,  $T$ ; were used as the dimensions of an ellipsoid as shown in Fig. 9. The volume of the ellipsoid was used to determine the diameter

of a sphere having the same volume as the ellipsoid. The diameter of this sphere,  $d_f$ , was termed the equivalent diameter of the largest fragment. The fragments produced when the  $t/D$  ratio was low tended to have length-to-diameter ratios of just less than one. The length-to-diameter ratio of the fragments with the higher  $t/D$  ratios tended towards values of 0.5 to 0.6. The large fragments in the external bubble of the test where the  $t/D$  ratio was 0.424, were very flaky, with length-to-diameter ratios of about 0.2.

\_\_\_\_\_

\_\_\_\_\_

---

\_\_\_\_\_

(b) (7)(C), (b) (7)(D)

---

\_\_\_\_\_

\_\_\_\_\_

1. \_\_\_\_\_

---

\_\_\_\_\_

---

---

---

\_\_\_\_\_

100



---

\_\_\_\_\_

1	2	3	4	5	6	7	8	9	10	11	12	13	14	15	16	17	18	19	20	21	22	23	24	25	26	27	28	29	30	31	32	33	34	35	36	37	38	39	40	41	42	43	44	45	46	47	48	49	50	51	52	53	54	55	56	57	58	59	60	61	62	63	64	65	66	67	68	69	70	71	72	73	74	75	76	77	78	79	80	81	82	83	84	85	86	87	88	89	90	91	92	93	94	95	96	97	98	99	100	101	102	103	104	105	106	107	108	109	110	111	112	113	114	115	116	117	118	119	120	121	122	123	124	125	126	127	128	129	130	131	132	133	134	135	136	137	138	139	140	141	142	143	144	145	146	147	148	149	150	151	152	153	154	155	156	157	158	159	160	161	162	163	164	165	166	167	168	169	170	171	172	173	174	175	176	177	178	179	180	181	182	183	184	185	186	187	188	189	190	191	192	193	194	195	196	197	198	199	200	201	202	203	204	205	206	207	208	209	210	211	212	213	214	215	216	217	218	219	220	221	222	223	224	225	226	227	228	229	230	231	232	233	234	235	236	237	238	239	240	241	242	243	244	245	246	247	248	249	250	251	252	253	254	255	256	257	258	259	260	261	262	263	264	265	266	267	268	269	270	271	272	273	274	275	276	277	278	279	280	281	282	283	284	285	286	287	288	289	290	291	292	293	294	295	296	297	298	299	300	301	302	303	304	305	306	307	308	309	310	311	312	313	314	315	316	317	318	319	320	321	322	323	324	325	326	327	328	329	330	331	332	333	334	335	336	337	338	339	340	341	342	343	344	345	346	347	348	349	350	351	352	353	354	355	356	357	358	359	360	361	362	363	364	365	366	367	368	369	370	371	372	373	374	375	376	377	378	379	380	381	382	383	384	385	386	387	388	389	390	391	392	393	394	395	396	397	398	399	400	401	402	403	404	405	406	407	408	409	410	411	412	413	414	415	416	417	418	419	420	421	422	423	424	425	426	427	428	429	430	431	432	433	434	435	436	437	438	439	440	441	442	443	444	445	446	447	448	449	450	451	452	453	454	455	456	457	458	459	460	461	462	463	464	465	466
---	---	---	---	---	---	---	---	---	----	----	----	----	----	----	----	----	----	----	----	----	----	----	----	----	----	----	----	----	----	----	----	----	----	----	----	----	----	----	----	----	----	----	----	----	----	----	----	----	----	----	----	----	----	----	----	----	----	----	----	----	----	----	----	----	----	----	----	----	----	----	----	----	----	----	----	----	----	----	----	----	----	----	----	----	----	----	----	----	----	----	----	----	----	----	----	----	----	----	-----	-----	-----	-----	-----	-----	-----	-----	-----	-----	-----	-----	-----	-----	-----	-----	-----	-----	-----	-----	-----	-----	-----	-----	-----	-----	-----	-----	-----	-----	-----	-----	-----	-----	-----	-----	-----	-----	-----	-----	-----	-----	-----	-----	-----	-----	-----	-----	-----	-----	-----	-----	-----	-----	-----	-----	-----	-----	-----	-----	-----	-----	-----	-----	-----	-----	-----	-----	-----	-----	-----	-----	-----	-----	-----	-----	-----	-----	-----	-----	-----	-----	-----	-----	-----	-----	-----	-----	-----	-----	-----	-----	-----	-----	-----	-----	-----	-----	-----	-----	-----	-----	-----	-----	-----	-----	-----	-----	-----	-----	-----	-----	-----	-----	-----	-----	-----	-----	-----	-----	-----	-----	-----	-----	-----	-----	-----	-----	-----	-----	-----	-----	-----	-----	-----	-----	-----	-----	-----	-----	-----	-----	-----	-----	-----	-----	-----	-----	-----	-----	-----	-----	-----	-----	-----	-----	-----	-----	-----	-----	-----	-----	-----	-----	-----	-----	-----	-----	-----	-----	-----	-----	-----	-----	-----	-----	-----	-----	-----	-----	-----	-----	-----	-----	-----	-----	-----	-----	-----	-----	-----	-----	-----	-----	-----	-----	-----	-----	-----	-----	-----	-----	-----	-----	-----	-----	-----	-----	-----	-----	-----	-----	-----	-----	-----	-----	-----	-----	-----	-----	-----	-----	-----	-----	-----	-----	-----	-----	-----	-----	-----	-----	-----	-----	-----	-----	-----	-----	-----	-----	-----	-----	-----	-----	-----	-----	-----	-----	-----	-----	-----	-----	-----	-----	-----	-----	-----	-----	-----	-----	-----	-----	-----	-----	-----	-----	-----	-----	-----	-----	-----	-----	-----	-----	-----	-----	-----	-----	-----	-----	-----	-----	-----	-----	-----	-----	-----	-----	-----	-----	-----	-----	-----	-----	-----	-----	-----	-----	-----	-----	-----	-----	-----	-----	-----	-----	-----	-----	-----	-----	-----	-----	-----	-----	-----	-----	-----	-----	-----	-----	-----	-----	-----	-----	-----	-----	-----	-----	-----	-----	-----	-----	-----	-----	-----	-----	-----	-----	-----	-----	-----	-----	-----	-----	-----	-----	-----	-----	-----	-----	-----	-----	-----	-----	-----	-----	-----	-----	-----	-----	-----	-----	-----	-----	-----	-----	-----

\_\_\_\_\_

---

\_\_\_\_\_

---

\_\_\_\_\_

---



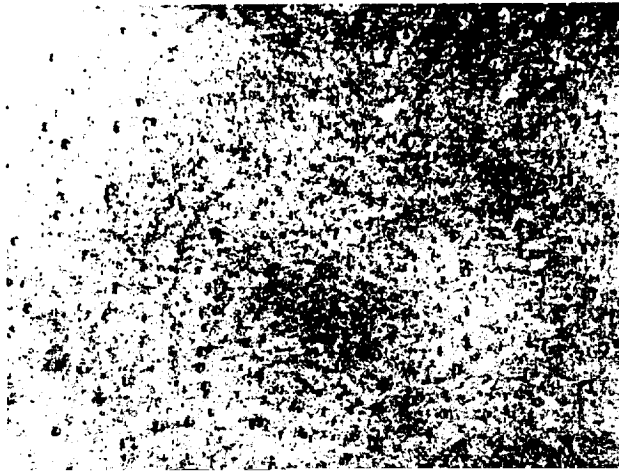
\_\_\_\_\_

\_\_\_\_\_

\_\_\_\_\_



Damage produced by the large fragments in the debris cloud shown in Fig. 8 is shown in Fig. 15. Impact of these fragments produced fairly large and deep craters over the entire surface of the 38-cm-square witness plate. Penetration resulting from the impact of a single fragment did not occur. However, local spall was produced on the rear of the plate below many of the larger craters. In the witness plate shown in Fig. 15, the diameter of the damage pattern produced by the projectile fragments was slightly smaller than for the test with  $t/D$  ratio of 0.234.



Understanding the debris cloud formation process for impact velocities beyond the current range of test capabilities, and the effects of the impact of this cloud on a rear wall, remain an issue of great interest. Analysis of select tests at velocities below 6.7 km/s will provide insights to debris cloud formation at velocities above 6.7 km/s.

Finally, a thorough understanding of the debris cloud formation at normal impact is required before meaningful study of the oblique impact is undertaken.

#### ACKNOWLEDGEMENT

The analytical effort described in this paper and a portion of the test program was performed under contract A71447 with Martin Marietta Manned Space System as a subcontract under prime contract NAS8-38856. The author wishes to gratefully acknowledge Dr. Normal Elfer of Martin Marietta and Mr. Joel Williamsen of Marshall Space Flight Center for their support of this work. He also wishes to express his appreciation to Mr. Burton Cour-Palais of McDonnell Douglas Space Systems Company for the use of his test results, and to Dr. Robert Schmidt of Boeing Defense and Space Group for providing several of the thinner 6061-T6 bumper sheet materials used in the tests.





